ORIGINAL ARTICLE

Seepage modelling and seepage-stress coupling properties of fractured rock mass based on equivalent circuit principle

Xiao Huang[1,2] · Jionghao Jin[1] · Chenlu Song[1] · Chong Shi[3] · Guoxiong Mei[2]

Abstract

The seepage-stress coupling characteristics of fractured rock mass were studied theoretically in this paper. Based on the cubic law and the equivalent circuit principle, a modified multi-parallel plate equivalent model (MPPEM) for seepage analysis of a rough single-fracture and a modified equivalent seepage resistance model (ESRM) for seepage analysis of a fracture networks consisting of rough single-fracture combined in series and parallel were proposed. On this basis, the equation for the variation of fracture aperture of fractured rock masses under the action of the three-direction principal stresses and pore water pressure was derived, and the discrete element calculations of the seepage-stress coupling of the two-dimensional fractured rock mass were carried out under different ground stress coefficients. The results show that the error of the modified MPPEM characterizing the seepage in a rough single-fracture in a rock mass does not exceed 7%. The modified ESRM can better characterize the seepage in T-shaped combined fracture and ×-shaped combined fracture. With the increase of normal stress applied to the fracture surface, the fracture aperture and seepage flow rate of the fractured rock mass decrease. The above study is of great theoretical significance for the analysis of the seepage evolution law of the fractured rock mass under the action of geostress.

Keywords Seepage · Fractured rock mass · Combined fracture · Seepage-stress coupling characteristics · Analytical model

Introduction

In the engineering construction of groundwater, oil, gas, and geothermal mining projects, the rock fractures are the main seepage channels in underground natural rock masses, and their seepage characteristics profoundly affect the mining efficiency and safety of those engineering projects (Neuman 2005). Meanwhile, the changes in stress and water pressure caused by the engineering disturbances will change the size and shape of the fracture cavity, which will lead to a change in the seepage characteristics (Crandall et al. 2010). Therefore, it is of great theoretical significance to carry out the research on the seepage-stress coupling characteristics of fractured rock masses to analyze the evolution characteristics of seepage field and the control of seepage variations in fractured rock masses in complex underground environments.

Fractured rock mass usually contains a large number of single fractures. A deep understanding of the seepage characteristics of single fractures is a prerequisite for understanding the hydro-mechanical coupling characteristics of fractured rock mass. In early studies, the single fracture in a rock mass, based on linear Darcy flow, was simplified into a smooth parallel plate model, and the classical cubic law was derived by solving the Navier–Stokes (N-S) equation to estimate the flow capacity of a single fracture (Dimadis et al. 2014; Brush and Thomson 2011). Considering the roughness of natural fracture surface, many researchers have modified the cubic law using mechanical apertures, equivalent hydraulic apertures, and parameters characterizing the roughness of the fracture surface (Barton et al. 1985; Hakami 1995; Waite et al. 1999; Xie et al. 2015). However, with the increase of flow velocity, the relationship between the water head difference at both ends of the fracture and the flow rate gradually

✉ Chenlu Song
  songchenlu@zjou.edu.cn

1. Department of Civil Engineering, Zhejiang Ocean University, Zhoushan 316022, China

2. Ocean College, Zhejiang University, Zhoushan 316021, China

3. Key Laboratory of Ministry of Education for Geomechanics and Embankment Engineering, Hohai University, Nanjing 210024, China

evolves into a nonlinear relationship (Zimmerman et al. 2004; Zhang and Nemcik 2013). To describe this nonlinear relationship, the Forchheimer equation was proposed (Bear 1972; Liu et al. 2016a, b), and the non-Darcy flow inertial coefficient in the equation was predicted (Javadi et al. 2010; Zhou et al. 2016; Liu et al. 2020). However, the Forchheimer equation is an empirical formula, and its applicability is relatively limited.

Compared to the critical role of roughness in single-fracture seepage, in the process of seepage in intersecting fractures and multi-fracture networks, factors such as fracture length, density, aperture, orientation, intersections, dead ends, etc. have a strong impact on the seepage properties of fractured rock masses (Jafari and Babadagli 2009; Jiang et al. 2014; Liu et al. 2016a, b). Considering the invisibility of the internal structure of natural rock fractures, effectively preparing experimental models and numerical network models with real and measurable fracture spatial geometries, and conducting seepage tests based on this to accurately estimate fluid flow behavior (Wang et al. 2016; Suzuki et al. 2017), remains a challenging problem. It is worth noting that through simplification of the fracture system, an ESRM based on analog circuit knowledge can effectively predict the seepage characteristics of fractured rock masses dominated by main fractures (Tao and Liu 2012; Liu et al. 2021).

For disturbed fractured rock masses, the complexity of the spatial geometry of the fracture system and the deformation induced by the stresses exerted on the fracture are the main reasons affecting the flow capacity of the fracture. Numerous scholars have conducted extensive experimental and theoretical studies on the deformation and seepage characteristics of rough rock fractures under normal and tangential stresses (Baghbanan and Jing 2008; Xue et al. 2014; Wang and Cardenas 2016; Jiang et al. 2022). A new laboratory technique with the coupled shear-flow tests of rock joints was developed by Esaki et al. (1999) and used to investigate the coupled effect on the joint shear deformation and dilatancy on the hydraulic conductivity of the rock joints. Zhou et al. (2015) investigated the nonlinear flow behavior at low Reynolds numbers through rough-walled fractures subjected to the normal compressive loading by laboratory tests. Wang et al. (2020a, b) conducted shear flow-tests with different roughness surfaces to explore the influence of the shear behavior on the hydraulic properties of rock fractures. Yang et al. (2022) employed the Comsol Multiphysics software to develop the hydro-mechanical coupling finite element model of the fracture networks with different intersection points under normal stress and shear stress, focusing on the influence of normal stress and shear stress on fracture permeability. However, all the above studies are mainly focusing on the seepage-stress coupling characteristics of the fractured rock masses under simple stress boundary conditions at laboratory scale.

In summary, the research on the seepage-stress coupling characteristics of rock mass containing rough single fracture has become relatively mature. For the seepage characteristics of rock mass with complex fracture system, scholars are more committed to constructing fractured rock mass close to the spatial characteristics of real rock mass fractures and carrying out corresponding laboratory tests and numerical simulation studies. However, the seepage evolution law of fractured rock mass is less analyzed from the theoretical level. Since the main cracks in the fractured rock mass have obvious distribution, their penetration degree, crack opening degree, and spanning area are more than the non-main cracks, and thus play a dominant role in the fracture seepage. Some scholars have simplified the fracture system in rock masses and proposed an equivalent seepage resistance model based on circuit knowledge (Tao and Liu 2012; Liu et al. 2021). The seepage characteristics of rock masses with regional main fractures are effectively predicted. However, these proposed equivalent circuit models assume that the fracture networks are smooth, which is inconsistent with the actual rock fracture networks Therefore, based on previous studies, this study further extends the seepage model of a fracture network composed of several rough single fractures through series and parallel connections. Firstly, based on the idea of local cubic law, the MMPEM of natural rough single fracture is constructed. Then, the seepage characteristics of cross fractures with different combinations of rough single fractures are analyzed by analogy circuit principle, and extended to two-dimensional rough fracture network. Finally, the seepage equations of fractured rock mass under the action of three-directional principal stresses and seepage water pressure are derived and verified by the discrete element method.

MPPEM for rough single-fracture seepage in rock mass and its modification

Single fracture is the basic element of fracture network in rock mass, and its seepage property is the basis of analyzing the seepage of fractured rock mass. As shown in Fig. 1, if a single fracture is regarded as two smooth parallel plates, the cubic law can be used to describe the flow of linear Darcy flow fluid in it (Dimadis et al. 2014). The volume flow q per unit width through the smooth parallel plate is obtained by simplifying the N-S equation (Ghia et al. 1982).

$$q = -\frac{b^3}{12\mu}\frac{\Delta P}{L} \tag{1}$$

where, b is the gap width of the parallel plate slit; ΔP is the pressure drop at both ends of the slit; μ is the dynamic viscous coefficient of the fluid; L is the flow length.
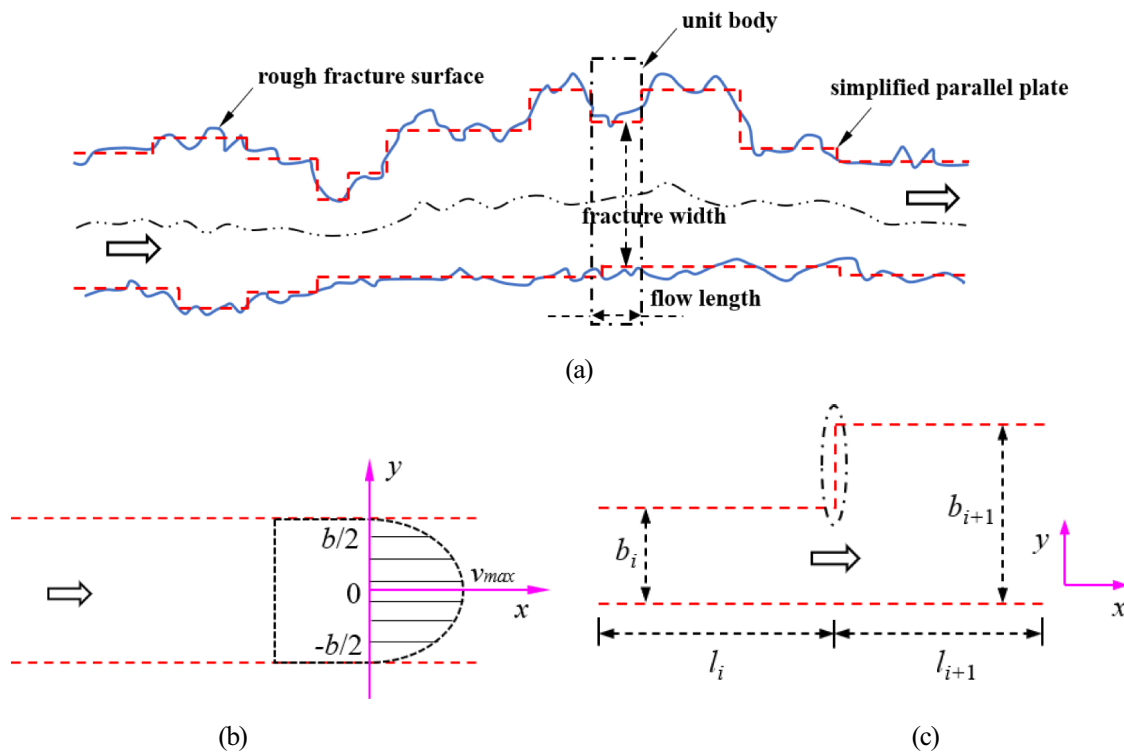
Fig. 1 Schematic of the local cubic law in rough single-fracture: **a** rough single-fracture multi-parallel plate model; **b** parallel plate model; **c** sudden change in gap width between adjacent parallel plates

MPPEM

Due to the uneven fracture wall of natural rock mass, the cubic law is obviously no longer applicable to describe the fluid flow in such rough fractures. Some scholars proposed a modified cubic law to analyze fluid flow in rough fractures by considering the geometric characteristics of the fractured walls. For instance, the roughness coefficient correction method, the frequency gap width representation method, and the contact area ratio method (Walsh 1981; Carlsson and Olsson 1993; Olsson and Barton 2001). These methods are all improvements on the cubic law, so they are only suitable for cracks with small fluctuation of gap width.

For most rock fractures, the fracture region with small fluctuation of gap width is the local fracture, that is, the local cubic law holds (Konzuk and Kueper 2004). Based on this, a MPPEM of rough single-fracture seepage is proposed. The core idea of the model is as follows: the whole rough fracture is discretized into a number of segments, so that the gap width fluctuation of each fracture segment is gentle, and the segmentation is the location of the relatively strong fluctuation of the gap width (Fig. 1(a)). When the number of discretized segments is sufficiently large, the discretized fracture segments converge to the original

fracture. The seepage in the discretized fracture segments can be described by the local cubic law, and the error due to the large fluctuation of the gap width in the segmentation is eliminated by the correction method.

The fluid flow in each parallel plate of rough single-fracture satisfies the cubic law, and the flow through each parallel plate is the same. Then, the pressure drop ΔP_i at both ends of the i-th parallel plate is

$$\Delta P_i = -\frac{12\mu q l_i}{b_i^3} \tag{2}$$

where, b_i and l_i are the aperture and length of the i-th parallel plate fracture segment, respectively.

The sum of the pressure drops at both ends of each parallel plate segment is equal to the pressure drop at both ends of the whole fracture, i.e., $\Delta P = \sum_{i=1}^{n} \Delta P_i$. When the number of fracture segments n is large enough, the discretized fractures approach the original fracture infinitely, meaning that the sum of all parallel plate lengths approximates the flow length of the whole fracture, i.e., $\sum_{i=1}^{n} l_i = L$. Therefore, the seepage expression for single-fracture based on the MPPEM is given by Eq. (3).

$$q = -\frac{1}{12\mu} \frac{\Delta P}{\sum_{i=1}^{n} (l_i/b_i^3)} = -\frac{1}{12\mu} \frac{\Delta P}{L} \frac{\sum_{i=1}^{n} l_i}{\sum_{i=1}^{n} (l_i/b_i^3)} \quad (3)$$

If the third multiplicative term in the above equation is denoted as the correction coefficient C, the expression is identical to the modified model based on the cubic law. It indicates that the MPPEM derived based on the idea of the local cubic law is feasible. Additionally, it should be noted that abrupt changes in aperture between adjacent parallel plates produces the excessive pressure drop loss (as shown in Fig. 1(c)), i.e., the actual pressure drop of the fluid at the location of aperture change is greater than the calculated value based on the local cubic law. To eliminate this error, an excess pressure drop loss coefficient is defined to correct the MPPEM.

Modification of the MPPEM

In order to analyze the additional pressure drop in the fluid due to sudden changes in the gap width, the excess pressure drop loss coefficient λ is defined as

$$\lambda = \Delta P_c / \Delta P \quad (4)$$

where, ΔP_c is the pressure drop calculated by the local cubic law; ΔP is the real measured pressure drop.

For the series parallel plates shown in Fig. 1(c), the theoretical pressure drop $\Delta(P_c)_i$ of the fluid through the i-th and $i+1$-th parallel plates is obtained from the local cubic law.

$$\Delta(P_c)_i = \Delta P_i + \Delta P_{i+1} = -12\mu q \left(\frac{l_i}{b_i^3} + \frac{l_{i+1}}{b_{i+1}^3} \right) \quad (5)$$

Substituting Eq. (4) into Eq. (5) yields the actual pressure drop of the fluid through the i-th and $i+1$-th parallel plates. By subtracting the actual pressure drop from the theoretical value, the pressure drop loss due to the fluctuation in gap width between the i-th and $i+1$-th parallel plates can be obtained. The sum of the theoretical pressure drop values for each parallel plate segment, added to the sum of the pressure

drop losses between adjacent parallel plates, gives the pressure drop of fluid flowing through a rough single fracture. After rearrangement, the modified MPPEM for rough single-fracture seepage is given by Eq. (6).

$$q = -\frac{1}{12\mu} \frac{\Delta P}{\sum_{i=1}^{n} \frac{l_i}{b_i^3} + \sum_{i=1}^{n-1} \left[\left(\frac{1}{\lambda_i} - 1 \right) \left(\frac{l_i}{b_i^3} + \frac{l_{i+1}}{b_{i+1}^3} \right) \right]} \quad (6)$$

The parameters directly related to the geometric characteristics of the fracture wall (such as the length and aperture of the parallel plate) in Eq. (6) can be obtained by arranging a series of measuring points on the natural fracture and dispersing them in sections. The excess pressure drop coefficient λ is determined through experimentation. According to the test results (Liu et al. 2021), the excess pressure drop coefficient for a contracting fracture ($b_i > b_{i+1}$) is significantly larger than that for an expanding fracture ($b_i < b_{i+1}$). The excess pressure drop coefficient for a contracting fracture under the condition of same lengths ($l_i = l_{i+1}$) of adjacent parallel plates satisfies Eq. (7).

$$\lambda_i = \frac{24\left[1 + \left(b_i/b_{i+1} \right)^3 \right]}{0.6 \text{Re}\left(b_i/l_i \right) + 28.28} \quad (7)$$

where, Re is the Reynolds number, and the Re of the test fluid is less than 1600.

Model validation

The modified MPPEM was verified using measured data of seepage through fractures with different roughness (Zhu 2012). The typical roughness curves of $4 \sim 6$ (JRC), $10 \sim 12$ (JRC) and $16 \sim 18$ (JRC) were selected for the test fractures. These three fracture curves were combined with the flat plate, and the fracture length was set to 100 mm, and the minimum fracture width was 0.51 mm, as shown in Fig. 2(a). By arranging a series of measurement points and discrete segments for each of the three fracture combinations, as

Fig. 2 Experimental model and theoretical model: **a** semi-rough and semi-flat fracture combination; **b** 6-P fracture dispersion diagram
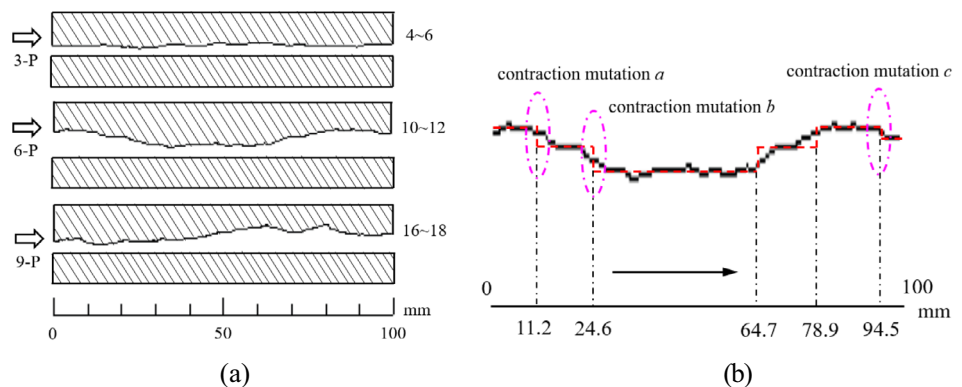
Table 1 Comparative analysis between theoretical value of model and test results

Fracture type	P_t/Pa	q_t/(10^{-3} m^{2}s^{-1})	Re	q_m/(10^{-3} m^{2}s^{-1})	Error (q_m)/%	λ_{av}	q_{vm}/(10^{-3} m^{2}s^{-1})	Error (q_{vm})/%
3-P	147.5	0.097	170	0.105	8	0.978	0.103	6
	49.2	0.034	60	0.035	3	0.983	0.0344	1
6-P	290.2	0.187	328	0.235	26	0.846	0.199	6
	149.0	0.106	186	0.117	10	0.932	0.109	3
9-P	49.8	0.120	207	0.143	19	0.897	0.128	7
	19.9	0.081	140	0.087	7	0.964	0.084	4

The subscript t denotes the laboratory test results, the subscript m represents the calculation results of the multi-parallel plate equivalent model, and the subscript vm denotes the calculation results of the modified multi-parallel plate equivalent model

Fig. 3 Fracture model and its mesh generation (simplified model of multi parallel plates): **a** Schematic diagram of geometric parameters of fracture model; **b** Mesh partitioning of the 6-P fracture model in local maps
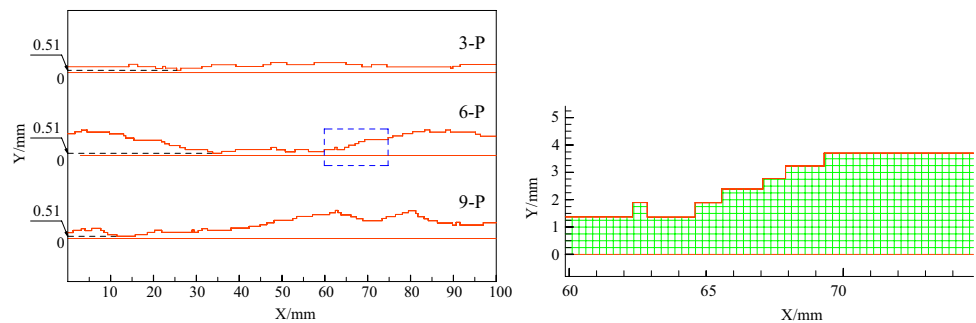
shown in Fig. 2(b), the theoretical value can be calculated by using the above formula.

The comparison between theoretical values and measured data is shown in Table 1. It can be seen from the table that the MPPEM can effectively characterize the seepage characteristics of the rough single fracture, with the seepage volume error not exceeding 26%. By introducing the excess pressure drop loss coefficient λ_{av}, the influence of multi-plate gap width mutation is significantly reduced, which makes the model accuracy further improved, with the error of the seepage volume not exceeding 7%.

Numerical calculations are conducted based on laminar viscosity model for three typical fractures in experimental works. Firstly, establish numerical models of fracture curves for 3-P, 6-P, and 9-P plates (fracture length 100 mm, minimum open width 0.51 mm), and import mesh partitioning grids (grid edge length is 0.25 mm), as shown in Fig. 3. The upper and lower boundaries of the numerical model are solid wall non slip boundaries, with the velocity inlet boundary on the left and the pressure outlet boundary on the right. Set the corresponding pressure difference according to the value of P_t in Table 1. The density of water is defined as 998.2 kg/m^3, and the dynamic viscosity is 0.0013 kg/m^3.

Figure 4 shows the distribution of flow lines in the local section of the 6-P fracture. It can be observed that the fluid flow line no longer maintains a parallel straight line due to the change in open width (expansion). It deviates towards the Y direction, and the degree of flow line deviation away from the tortuous open width is smaller; The expansion of
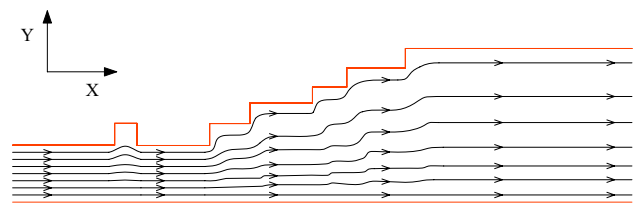

Fig. 4 Streamline of 6-P fracture ($P_t = 149.0$ Pa)

open width causes the fluid streamline to loosen and the flow velocity decreased. The comparison between the theoretical and numerical results of the flow rate model with several parallel plates and vertical connections between the plates for rough fracture treatment is shown in Fig. 5. The numerical results based on the Navier Stokes equation are very close to the theoretical results, and the applicability of the method based on local cubic law is verified.

Modified ESRM for combined fracture seepage in rock mass

In fractured rock mass, there are a few cases of single fracture penetrating. From the perspective of fracture combination, rock mass fracture is a fracture system composed of several single fractures (Barton et al 1985). The most basic connection modes between single fractures can be divided into series and parallel, as shown in Fig. 6. In the following,
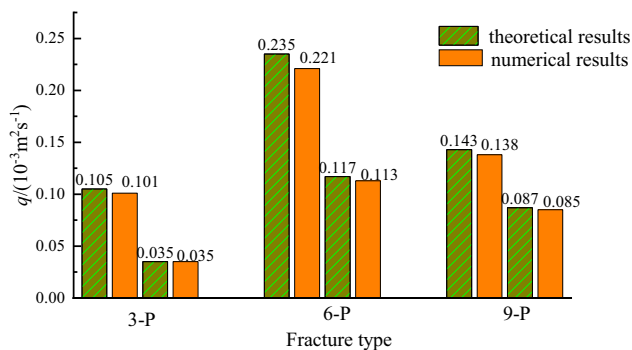
Fig. 5 Comparison between theoretical and numerical results of flow in different fractures
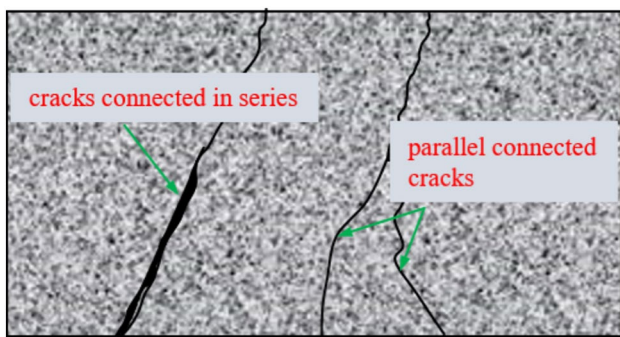

Fig. 6 Schematic diagram of basic combination relationship of fractures

the seepage characteristics of the combined fractures of these two combination methods are respectively studied.

For the convenience of analysis, the rough single fracture is equivalently treated as a parallel plate to which the cubic law applies. The equivalent gap width b_{eq} of the parallel plate slit after the equivalent treatment, i.e., the equivalent aperture of the rough single fracture, is given by Eq. (8).

$$b_{eq} = \sqrt[3]{\frac{\sum_{i=1}^{n} l_i}{\sum_{i=1}^{n} \frac{l_i}{b_i^3} + \sum_{i=1}^{n-1} \left[\left(\frac{1}{\lambda_i} - 1 \right) \left(\frac{l_i}{b_i^3} + \frac{l_{i+1}}{b_{i+1}^3} \right) \right]}} \quad (8)$$
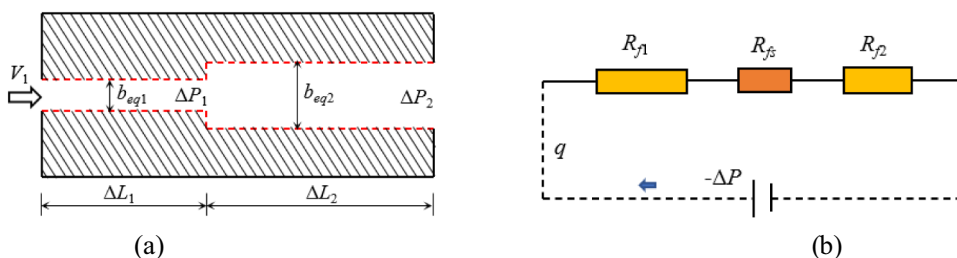
ESRM for series fracture seepage and its modification

The series fracture is treated as two segments of equivalent parallel plates with different gap widths, as shown in Fig. 7(a). The flow through the two segments of different gap widths of the equivalent parallel plates is the same. The sum of the pressure drops of the fluid flowing through the two parallel plate segments is the total pressure drop ΔP for the series fracture.

$$-\Delta P = q \left(\frac{12\mu\Delta L_1}{b_{eq1}^3} + \frac{12\mu\Delta L_2}{b_{eq2}^3} \right) \quad (9)$$

where, b_{eq1} and b_{eq2} are the gap widths of the two equivalent parallel plates, respectively; ΔL_1 and ΔL_2 are the lengths of the two equivalent parallel plates, respectively.

In analog circuits, the resistors are connected in series, which satisfies the formula $U = I(R_1 + R_2)$. This formula is similar in structure to Eq. (9). It can be seen that $-\Delta P$ is analogous to the voltage U, q is analogous to the current I, and $12\mu\Delta L/b_{eq}^3$ is analogous to the resistance R. Therefore, Eq. (9) can also be expressed as $-\Delta P = q(R_{f1} + R_{f2})$, where R_f represents equivalent seepage resistance.

The pressure drop loss of fluid through a series fracture formed by two equivalent parallel plates with different gap widths cannot be ignored because of the extra pressure drop caused by the sudden change of gap width. Therefore, the ESRM of series fracture should be modified. In the above analysis, the total pressure drop of adjacent parallel plates is treated as the sum of pressure drop of two parallel plates plus the pressure drop loss caused by the change of gap width. Because the flow q is constant, the total equivalent seepage resistance of the series fracture is equal to the sum of the equivalent seepage resistance of the two equivalent parallel plates (R_{f1} and R_{f2}) plus the equivalent seepage resistance loss R_{fs} caused by the change of gap width, as shown in Fig. 7(b). The equation of the modified ESRM is $-\Delta P = q(R_{f1} + R_{f2} + R_{fs})$.

Using the excess pressure drop loss coefficient λ proposed above (assuming $\Delta L = \Delta L_1 = \Delta L_2$), the equivalent seepage resistance loss R_{fs} is solved to obtain Eq. (10). Furthermore,

Fig. 7 Seepage modeling of equivalent parallel plate fractures connected in series: **a** seepage diagram of series fracture; **b** series equivalent circuit diagram

(a)

(b)

the expression of the modified ESRM of the series fracture can be derived.

$$R_{fs} = \frac{1-\lambda}{\lambda}\left(R_{f1} + R_{f2}\right) \tag{10}$$

$$q = -\frac{24\left[1 + \left(b_{eq1}/b_{eq2}\right)^3\right]}{0.6\mathrm{Re}\left(b_{eq1}/\Delta L\right) + 28.28} \frac{\Delta P}{\frac{12\mu\Delta L}{b_{eq1}^3} + \frac{12\mu\Delta L}{b_{eq2}^3}} \tag{11}$$

Considering the series fracture in Fig. 7 as a unit body and generalizing to the network of multiple series fractures shown in Fig. 8, there are

$$q = \frac{-\Delta P}{\sum_i \left(R_{f1} + R_{fs} + R_{f2}\right)_i} = \frac{-\Delta P}{\sum_i \left(R_{f1} + R_{f2}\right)_i \Big/ \lambda_i} \tag{12}$$

where, subscript i is the i-th unit body.

ESRM for parallel fracture seepage

The parallel fracture is treated as two equivalent parallel plates with different gap widths connected in parallel, as shown in Fig. 9. The total flow through the parallel fracture is the sum of the flow through each branch fracture. In the parallel fracture, the total pressure drop after the fluid flows is equal to the pressure drop through each branch fracture., i.e., $\Delta P = \Delta P_1 = \Delta P_2$. Then, Eq. (13) is obtained.

$$q = \frac{-\Delta P}{12\mu\Delta L_1 \Big/ b_{eq1}^3} + \frac{-\Delta P}{12\mu\Delta L_2 \Big/ b_{eq2}^3} = \frac{-\Delta P}{R_{f1}} + \frac{-\Delta P}{R_{f2}} \tag{13}$$

In analog circuits, resistors in parallel satisfy the formula $I = U/R_1 + U/R_2$, which is very similar to Eq. (13) in the structure of the expression, indicating that mathematical relationships similar to those in parallel circuits exist in parallel fracture seepage. There is no sudden change in gap width and no pressure drop loss in the parallel fracture. Consequently, Eq. (13) is the expression for the ESRM for parallel fracture seepage. Further generalization of the parallel fracture to a network of multiple parallel fractures as shown in Fig. 10, Eq. (14) can be obtained.

$$q = \frac{-\Delta P}{\frac{1}{\sum_j 1/R_{fj}}} = -\Delta P \sum_j 1/R_{fj} \tag{14}$$

where, subscript j is the j-th fracture in the parallel fracture network.

Seepage equations of typical series–parallel combined fractures

There are many ways of series–parallel combination of fractures, and one of the typical combined fractures is T-shaped fracture, as shown in Fig. 11(a). In the figure, crack A is connected in series with cracks B and C, while cracks B and C are connected in parallel. There are two

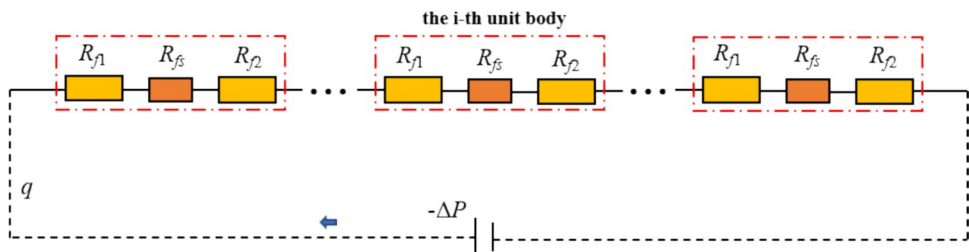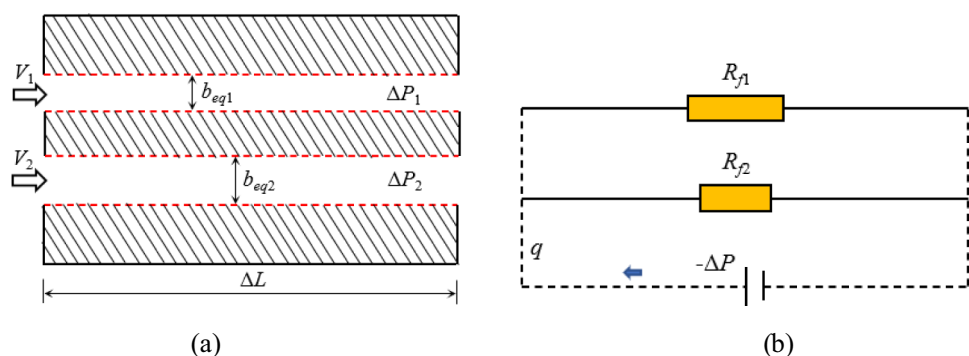**Fig. 8** Equivalent parallel plate seepage in a network of multiple series fractures

Fig. 9 Seepage modeling of equivalent parallel plate fractures connected in parallel: **a** seepage diagram of parallel fracture; **b** schematic of the parallel equivalent circuit
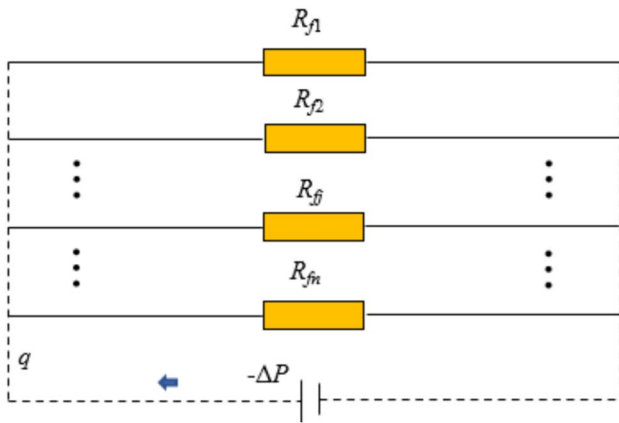
Fig. 10 Equivalent parallel plate seepage in a network of multiple parallel fractures

gap width mutations in the T-shaped fracture, which are located in series fracture A-B and series fracture A-C, respectively. The series fracture A-B is affected by crack C, and the equivalent seepage resistance loss R_{fs2} of the series fracture A-B can be obtained by considering the relationship between Reynolds number and flow (Liu et al. 2021). In the same way, the equivalent seepage resistance loss R_{fs3} of the series fracture A-C can be obtained. The seepage equations for the T-shaped combined fracture can

be derived based on the equivalent circuit characteristics in Fig. 11(b).

$$R_{fs2} = \left\{ \frac{0.6b_{eq2}\mathrm{Re}\left/\left[\Delta L\left(b_{eq3}^3\left/b_{eq2}^3 + 1\right)\right]\right. + 28.28}{24\left(b_{eq2}^3\left/b_{eq1}^3 + 1\right)\right.} - 1 \right\}\left(R_{f1} + R_{f2}\right)$$

$$R_{fs3} = \left\{ \frac{0.6b_{eq3}\mathrm{Re}\left/\left[\Delta L\left(b_{eq2}^3\left/b_{eq3}^3 + 1\right)\right]\right. + 28.28}{24\left(b_{eq3}^3\left/b_{eq1}^3 + 1\right)\right.} - 1 \right\}\left(R_{f1} + R_{f3}\right)$$

$$q = \frac{-\Delta P}{R_{f1} + \frac{(R_{f2}+R_{fs2})(R_{f3}+R_{fs3})}{(R_{f2}+R_{fs2})+(R_{f3}+R_{fs3})}}$$

(15)

The ×-shaped combined fracture is another typical model for series–parallel combined fractures, illustrated in Fig. 12. This model consists of two intersecting fractures with varying equivalent gap widths ($b_{eq1} > b_{eq2}$) and an angle θ between them. The pore water pressures at the left and right ends of the fractures are ΔP and 0, respectively. When neglecting the angle θ between the fractures, the ×-shaped combined fractures can be regarded as a parallel combination of fractures A-B on the left side and a parallel combination of fractures C-D on the right side, interconnected in series at the intersection point.

Fig. 11 Equivalent parallel plate flow in T-shaped combined fracture: **a** diagram of flow in T-shaped combined fracture; **b** equivalent circuit diagram of T-shaped combined fracture
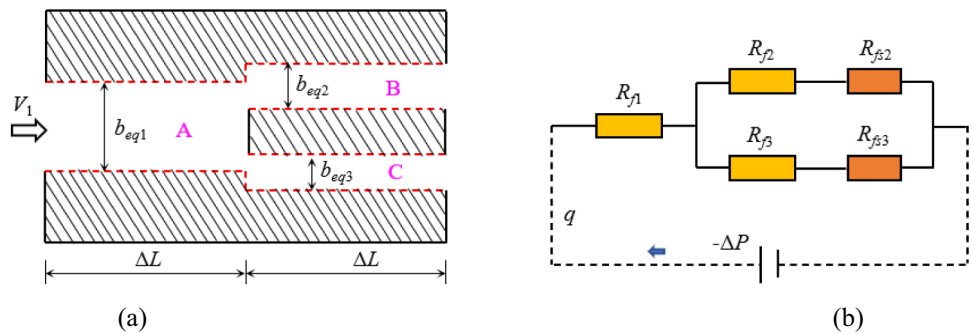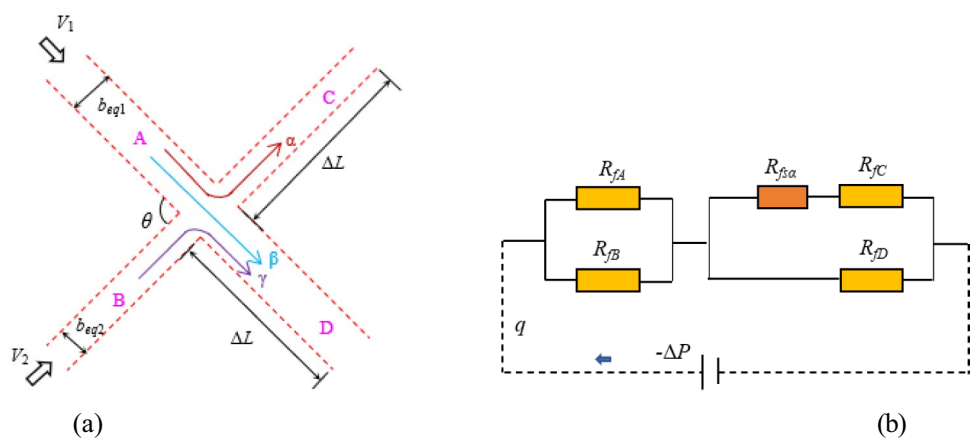

Fig. 12 Equivalent parallel plate flow in ×-shaped combined fracture: **a** diagram of flow in ×-shaped combined fracture; **b** equivalent circuit diagram of ×-shaped combined fracture

According to the results of cross-fractures seepage [Zhu 2012], the fluid in the cross-fractures can be divided into three strands: α-fluid that enters the narrow fracture from the wide fracture through the intersection point, β-fluid that enters the wide fracture from the wide fracture through the intersection point, and γ-fluid that enters the wide fracture from the narrow fracture through the intersection point. Obviously, only α-fluid passes through the gap width contraction, and thus the pressure drop loss needs to be considered.

According to the equivalent seepage resistance model of series and parallel fractures, combined with the equivalent circuit diagram shown in Fig. 12(b), the seepage equation of the $\times$-shaped combined fracture can be obtained.

$$R_{f1} = R_{f4} = \frac{12\mu\Delta L}{b_{eq1}^3}, \quad R_{f2} = R_{f3} = \frac{12\mu\Delta L}{b_{eq2}^3}$$

$$R_{fs\alpha} = \left(R_{f1} + R_{f3}\right)\left(\frac{0.6\text{Re}_4\left(b_{eq2}\big/\Delta L\right) + 28.28}{24\left[1 + \left(b_{eq2}\big/b_{eq1}\right)^3\right]} - 1\right) \tag{16}$$

$$q = -\Delta P \frac{1}{\left(\frac{1}{\frac{1}{R_{f1}} + \frac{1}{R_{f2}}} + \frac{1}{R_{fs\alpha} + R_{f3}} + \frac{1}{R_{f4}}\right)}$$

where, R_{f1}, R_{f2}, R_{f3} and R_{f4} are the equivalent seepage resistances of fractures A, B, C, and D, respectively, and $R_{fs\alpha}$ is the equivalent seepage resistance loss of α-fluid passing through the gap width contraction.

Hydro-mechanical coupling characterization of two-dimensional rough fracture networks

Theoretical model

The investigation of fracture aperture variation in response to external forces is crucial for understanding seepage in fractured rock masses. This section focuses on analyzing the influence of stress-induced deformation on fractures and rock blocks, which subsequently affects the seepage behavior. The rock mass consists of n-1 parallel fractures with uniform aperture. The fractures exhibit normal deformation stiffness in the x-direction, denoted as K_{nx}. Moreover, the fractured rock mass is subjected to pore pressure Δp, along with principal stresses $\Delta\sigma_x$, $\Delta\sigma_y$, and $\Delta\sigma_z$ in three directions, as illustrated in Fig. 13 In the analysis, the seepage coefficient of the rock blocks, which is considerably smaller than that of the fractures, is considered negligible to simplify calculations.

The displacement of rock mass in the x-direction, Δu_{tx}, is the sum of the displacement of fractures, Δu_{fx}, and the

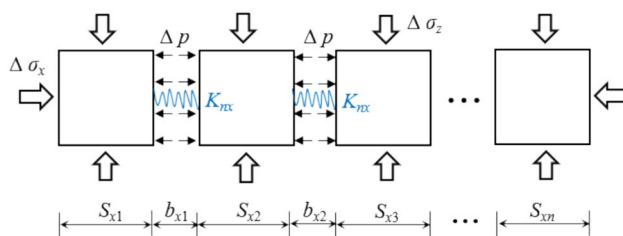**Fig. 13** Analytical model of fractured rock mass under the action of principal stress and pore water pressure

displacement of rock blocks, Δu_{fx}. Therefore, the displacement of fractures, Δu_{fx}, can be expressed as

$$\Delta u_{fx} = \Delta u_{tx} - \Delta u_{rx} = \left(S_x + b_x\right)\Delta\varepsilon_{tx} - S_x\Delta\varepsilon_{rx} \tag{17}$$

where, S_x and b_x are the sum of the widths of rock blocks and fractures along the x-direction, respectively, i.e., $S_x = \sum S_{xi}$, $b_x = \sum b_{xi}$; $\Delta\varepsilon_{tx}$ and $\Delta\varepsilon_{rx}$ are the strains of the rock mass and rock blocks along the x-direction, respectively.

Under the action of three-dimensional principal stress and pore pressure, the rock mass strain $\Delta\varepsilon_{tx}$ and rock block strain $\Delta\varepsilon_{rx}$ along the x-direction can be expressed as Eq. (18). Furthermore, the variation of rock fracture aperture Δu_{fx} is derived as Eq. (19).

$$\begin{aligned}
\Delta\varepsilon_{tx} &= \frac{1}{E_{tx}}\left[\Delta\sigma_x - v\left(\Delta\sigma_y + \Delta\sigma_z\right)\right] \\
\Delta\varepsilon_{rx} &= \frac{1}{E_{rx}}\left[\Delta\sigma_x + \Delta p - v\left(\Delta\sigma_y + \Delta\sigma_z\right)\right]
\end{aligned} \tag{18}$$

where, E_{tx} is the elastic modulus of the rock mass, which is related to the elastic modulus of the rock blocks (E_{rx}) and the normal stiffness of the fractures (K_{nx}); v is the Poisson's ratio. According to the series connection relationship, it can be inferred that $1/E_{tx} = 1/E_{rx} + 1/S_x K_{nx}$.

$$\Delta u_{fx} = \left[\frac{\left(S_x + b_x\right)\left(S_x K_{nx} + E_{rx}\right)}{E_{rx}S_x K_{nx}} - \frac{S_x}{E_{rx}}\right]$$
$$\left[\Delta\sigma_x - v\left(\Delta\sigma_y + \Delta\sigma_z\right)\right] - \frac{S_x\Delta p}{E_{rx}} \tag{19}$$

In Fig. 13, the aperture b'_{xj} of the j-th fracture after the action of the three-way principal stress and the pore pressure is Eq. (20). Combined with the seepage equation of the network of multiple parallel fractures (Eq. (14)), the seepage equation of the network of multiple parallel fractures under the action of three-way principal stress and pore pressure can be obtained (Eq. (21)).

$$b'_{xj} = b_{xj}\left\{1 - \frac{\left[\frac{(S_x+b_x)(S_x K_{nx}+E_{rx})}{E_{rx}S_x K_{nx}} - \frac{S_x}{E_{rx}}\right]\left[\Delta\sigma_x - v\left(\Delta\sigma_y + \Delta\sigma_z\right)\right] - \frac{S_x\Delta p}{E_{rx}}}{b_x}\right\} \tag{20}$$

$$q = -\Delta P \sum_j \left[\left(b'_{xj} \right)^3 \Big/ 12\mu\Delta L \right] \qquad (21)$$

Validation

The stress-seepage analysis was performed by Matlab as shown in Fig. 14(a). There are three parallel fractures in the rock mass, with a width of each fracture $b_{xj} = 0.1$ mm. The height of the rock sample is $\Delta L = 40$ mm, and the width of a single rock block is $S_{xj} = 5$ mm. The other parameter values were set as follows: rock thickness $a = 10$ mm (flow cross-section $A = a \cdot b_x$), fluid viscosity coefficient $\mu = 1.14 \times 10^{-3}$ N·s/m², Poisson's ratio $v = 0.2$, elastic modulus of rock blocks $E_{rx} = 500$ MPa, normal stiffness of fractures $K_{nx} = 10^4$ MPa/m, and pore water pressure $\Delta p = 1$ MPa. For the convenience calculation, the load was only applied in the direction of normal stress σ_x on the fractures.

The relationship between seepage, equivalent seepage resistance, and stress increment is shown in Fig. 14(b). The seepage of the fractured rock mass decreases exponentially with the normal stress increasing on the fracture surfaces, which is consistent with experimental results. Furthermore, it is also observed that the equivalent seepage resistance of the fractured rock mass increases exponentially with the normal stress increasing on the fracture surfaces, which is consistent with previous research findings (Peng et al. 2003; Jafari and Babadagli 2009).

Seepage-stress coupling analysis of fracture networks by UDEC

The UDEC program has proven to be a suitable tool for conducting stress-seepage coupled analysis on fracture networks (Wang et al. 2020a, b). In this analysis, rock blocks intersected by fractures are simulated as either rigid or deformable bodies. The seepage within the fractures is then simulated by modeling fluid flow between these blocks. Figure 15 showcases the numbered domains, ranging from 1 to 5, with the assumption that each domain is filled with isotropic fluid under equal pressure. These domains interact through contacts or interfaces, and their contact order is designated as A to F. Domains 1, 3, and 4 represent the fractures themselves, while domain 2 corresponds to the intersection point of two fractures, and domain 5 represents a cavity. The pressure difference between adjacent domains induces fluid flow.

Assuming that only the normal stress acting on the fracture surface is present in Eq. (20), the increment of hydraulic aperture Δb is linearly related to the increment of normal stress $\Delta\sigma_n$, and the increment of pore pressure Δp is the multiplicative term in this linear relationship. The initial hydraulic aperture is denoted as b_0, then the increment of

Fig. 14 Fractured rock sample and seepage results: **a** schematic of fractured rock samples (in mm); **b** relationship between seepage, equivalent seepage resistance, and stress increment
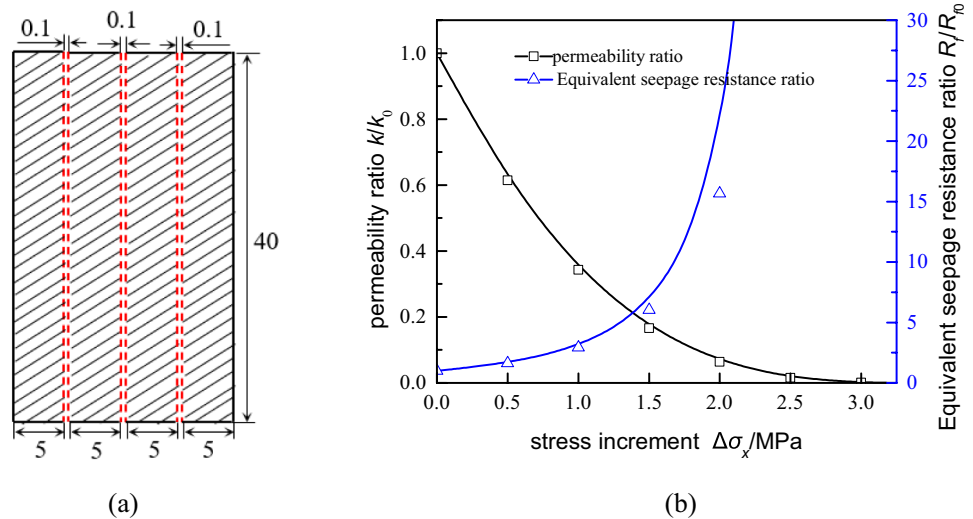

(a)

(b)

Fig. 15 Fluid flow model in UDEC and the relationship between gap width and normal stress: **a** inter-domain flow in fracture; **b** linear relationship between fracture aperture and normal stress
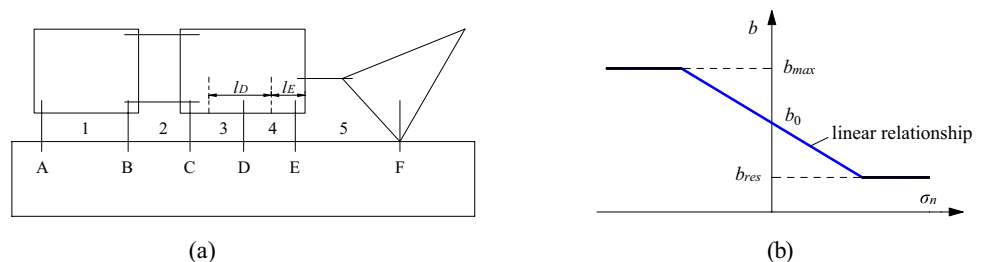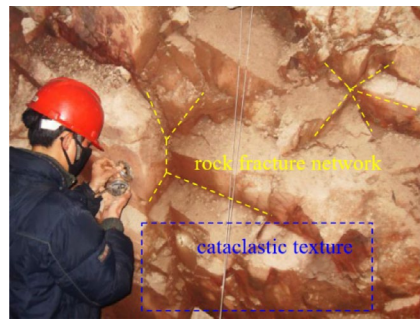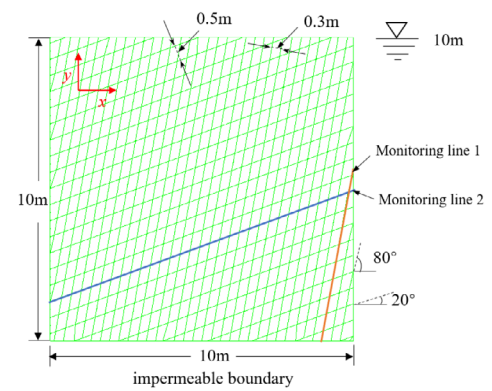

(a)

(b)

Fig. 16 Numerical model of a rock fracture network: **a** fractured surrounding rock of main powerhouse; **b** simplified fracture network in rock mass

(a)

(b)

Table 2 Physical and mechanical parameters of rock blocks

Density/ g·cm^{-3}	Young's modulus/ GPa	Poisson's ratio	Cohesion/ MPa	Internal friction angle/º	Tensile strength/ MPa
2600	13.9	0.26	4.6	45	2.89

Table 3 Physical and mechanical parameters of joints

Normal stiffness /GPa	Tangential stiffness /GPa	Tensile strength /MPa	Cohesion/ MPa	Internal friction angle/º
4.6	3.4	0.1	0.2	32

normal aperture under a certain normal stress condition can be expressed as $u_n = u(b_0, \Delta\sigma_n, \Delta p)$. Consequently, the hydraulic aperture b can be further defined by Eq. (22), which can be embedded in the UDEC.

$$b = b_0 + u_n = b_0 + u(b_0, \Delta\sigma_n, \Delta p) \qquad b_{res} \le b \le b_{max} \tag{22}$$

To analyze the seepage characteristics of fractured rock masses under different stress conditions, this study conducted simulations to investigate the variations in pore pressure, seepage velocity, and fracture aperture for different in-situ stress ratios (σ_x/σ_y). According to the rock structure characteristics of the fractured surrounding rock of the mainhouse of Liyang Pumped Storage Power Station in China, the numerical model of the fractured rock mass shown in Fig. 16 was established. The model incorporated two sets of fractures, oriented at 20° and 80° with respect to the *x*-direction, each with respective fracture spacing of 0.5 m and 0.3 m. The left and right boundaries of the model were horizontally fixed. At the left boundary, a water pressure of 0 was imposed, while at the right boundary, a hydraulic gradient of 10 m head (0.1 MPa) was applied. The model's bottom was impermeable and fixed. Table 2 and Table 3 provide the computational parameters for the rock blocks and fractures, respectively. Regarding fluid calculation parameters, the density was set at 1000 kg/m³, the seepage coefficient at 10^8 MPa^{-1} s^{-1}, the initial aperture at 2×10^{-4} m, and the residual aperture at 5×10^{-5} m. The in-situ stress ratios examined were 0.25, 1.0, 1.5, and 2.0. The analysis focused on assessing the variations in seepage under different horizontal stress conditions, while maintaining the vertical stress constant.

Figure 17 illustrates the changes in pore pressure, seepage velocity, and fracture aperture with the in-situ stress ratio (horizontal stress). The observations are as follows: (a) The pore pressure within the fractured rock mass is higher in the lower-right region, influenced by the horizontal hydraulic gradient and gravity, while it is lower in the upper-left region. There is minimal variation in the pore pressure as the in-situ stress ratio increases, with a maximum value of approximately 0.09918 MPa. (b) The seepage velocity is higher in the lower-left region of the fractured rock mass, predominantly occurring in fractures inclined at 20° to the horizontal direction. The seepage velocity decreases continuously as the in-situ stress ratio increases from 0.25 to 2.0, ranging from 0.124 m/s to 0.1024 m/s. (c) The hydraulic aperture in the upper region of the fractured rock mass is larger than that in the lower region due to the linear increase of horizontal stress with burial depth. The difference in hydraulic aperture between the upper and lower regions is further amplified with an increase in the in-situ stress ratio. The hydraulic aperture of the fractured rock mass decreases continuously with an increasing in-situ stress ratio, decreasing from a maximum aperture of 2.052×10^{-4} m at an in-situ stress ratio of 0.25 to a reduced aperture of 2.024×10^{-4} m at an in-situ stress ratio of 2.0. Consequently, the fracture aperture and seepage velocity of the fractured rock mass decrease with an increase in horizontal stress, aligning with previous research findings (Peng et al. 2003).

Fig. 17 Seepage results of fractured rock mass under different in-situ stress coefficient: **a** $K = 0.25$; **b** $K = 1.0$; **c** $K = 1.5$; **d** $K = 2.0$
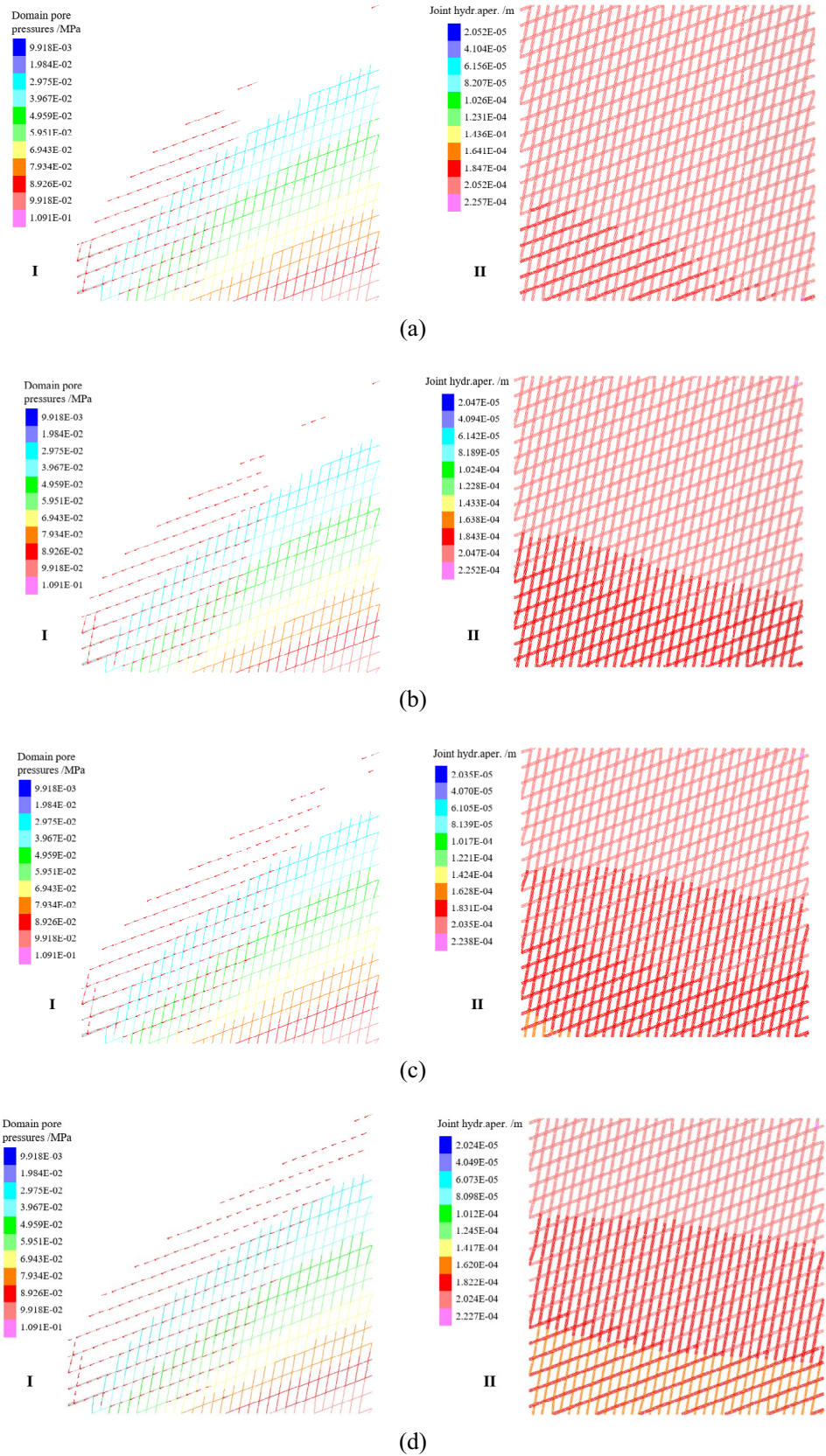
Conclusions

The fracture network within the rock mass was considered as a fracture system composed of multiple rough single-fractures combined in series and parallel. To describe the seepage properties of the rough single-fracture and analyze the seepage properties of the combined fracture, a modified MPPEM and a modified ESRM were proposed, respectively. The local cubic law and the principle of analog circuit serve as the basis for these models. Additionally, an equation for the seepage evolution of the fractured rock mass was derived, taking into account the influence of principal stress and pore pressure. The study also investigated the variations in fracture aperture, pore pressure, and flow velocity of the fractured rock mass under different ground stress coefficients.

(1) The rough single-fracture was discretized into a series-connected fracture segments with smooth fluctuations in gap width. The seepage in the discretized fracture segments was described by the local cubic law, and the error caused by large fluctuations in the gap width at the segments was reduced by the introduction of an excess pressure drop loss coefficient. This modified MPPEM can effectively characterize the seepage in a rough single-fracture, and the error of the seepage amount does not exceed 7%.

(2) The main fracture within the fractured rock mass can be conceptualized as a number of single-fractures in series and the parallel combination of the fracture system. The seepage behavior can be analogously described using circuit principles. The total equivalent seepage resistance of the series combination fracture is the sum of the equivalent seepage resistance of the two parallel plates, along with the additional equivalent seepage resistance loss (R_{fs}) caused by changes in gap width. In contrast, the parallel combination fracture does not exhibit gap width variations or pressure drop losses. The modified ESRM effectively captures the seepage characteristics of both T-shaped and ×-shaped combined fractures and can be broadly applied to analyze two-dimensional rough fracture networks.

(3) The equations for the variation of fracture aperture of the fracture network in a fracture rock mass considering the effects of three-directional principal stresses and pore water pressure are derived. Discrete element calculations of seepage-stress coupling in the fractured rock mass under different ground stress coefficients show that fracture aperture and seepage flow rate of the fractured rock mass decrease with the increase of horizontal compressive stress.

Author contributions Xiao Huang: Conceptualization, Methodology, Software, Validation, Formal analysis, Data curation, Writing—original draft, Writing—review & editing. Jionghao Jin: Formal analysis, Data curation, Writing—review & editing. Chenlu Song: Conceptualization, Formal analysis, Writing—review & editing. Chong Shi: Software, Funding acquisition. Guoxiong Mei: Conceptualization, Writing—review & editing.

Data availability All data generated or analysed during this study are included in this article.

Declarations

Conflict of interest The authors declare that they have no known competing financial interests or personal relationships that could have appeared to influence the work reported in this paper.

References

Baghbanan A, Jing L (2008) Stress effects on permeability in a fractured rock mass with correlated fracture length and aperture. Int J Rock Mech Min Sci 45:1320–1334. https://doi.org/10.1016/j.ijrmms.2008.01.015

Barton N, Bandis S, Bakhtar K (1985) Strength, deformation and conductivity coupling of rock joints. Int J Rock Mech Min Sci Geomech Abstr 22:121–140. https://doi.org/10.1016/0148-9062(85)93227-9

Bear J (1972) Dynamics of Fluids in Porous Media. Elsevier Pub. Co., New York

Brush DJ, Thomson NR (2011) Fluid flow in synthetic rough-walled fractures: Navier-Stokes, Stokes, and local cubic law simulations. Water Resour Res 39:1037–1041. https://doi.org/10.1029/2002WR001346

Carlsson A, Olsson T (1993) The analysis of fractures, stress and water flow for rock engineering projects. Anal Des Methods 1993:415–437. https://doi.org/10.1016/B978-0-08-040615-2.50023-X

Crandall D, Bromhal G, Karpyn ZT (2010) Numerical simulations examining the relationship between wall-roughness and fluid flow in rock fractures. Int J Rock Mech Min Sci 47:784–796. https://doi.org/10.1016/j.ijrmms.2010.03.015

Dimadis G, Dimadi A, Bacasis I (2014) Influence of Fracture Roughness on Aperture Fracture Surface and in Fluid Flow on Coarse-Grained Marble, Experimental Results. J Geosci Environ Prot 2:59–67. https://doi.org/10.4236/gep.2014.25009

Esaki T, Du S, Mitani Y et al (1999) Development of a shear-flow test apparatus and determination of coupled properties for a single rock joint. Int J Rock Mech Min Sci 36:641–650. https://doi.org/10.1016/S0148-9062(99)00044-3

Ghia U, Ghia KN, Shin CT (1982) High-Re solutions for incompressible flow using the Navier-Stokes equations and a multigrid method. J Comput Phys 48:387–411. https://doi.org/10.1016/0021-9991(82)90058-4

Hakami E (1995) Aperture distribution of rock fractures. Royal Institute of Technology, Stockholm

Jafari A, Babadagli T (2009) A sensitivity analysis for effective parameters on 2D fracture-network permeability. Spe Reserv Eval Eng 12:455–469. https://doi.org/10.2118/113618-PA

Javadi M, Sharifzadeh M, Shahriar K (2010) A new geometrical model for non-linear fluid flow through rough fractures. J Hydrol 389:18–30. https://doi.org/10.1016/j.jhydrol.2010.05.010

Jiang YJ, Li B, Wang CS et al (2022) Advances in development of shear-flow testing apparatuses and methods for rock fractures: A review. Rock Mech Bull 1:1–28. https://doi.org/10.1016/j.rockmb.2022.100005

Jiang MZ, Zhao GF, Bai NY, et al (2014) Research on the law of hydraulic fracture and natural fracture intersecting extension in the heterogeneous fractured reservoir. J Chem Pharm Res 6:816–820. https://api.semanticscholar.org/CorpusID:204954963

Konzuk JS, Kueper BH (2004) Evaluation of cubic law based models describing single-phase flow through a rough-walled fracture. Water Resour Res 40:1–17. https://doi.org/10.1029/2003WR002356

Liu R, Jiang Y, Li B (2016a) Effects of intersection and dead-end of fractures on nonlinear flow and particle transport in rock fracture networks. Geosci J 20:415–426. https://doi.org/10.1007/s12303-015-0057-7

Liu R, Li B, Jiang Y (2016b) Critical hydraulic gradient for nonlinear flow through rock fracture networks: the roles of aperture, surface roughness, and number of intersections. Adv Water Resour 88:53–65. https://doi.org/10.1016/j.advwatres.2015.12.002

Liu XS, Li M, Zeng ND et al (2020) Investigation on nonlinear flow behavior through rock rough fractures based on experiments and proposed 3-dimensional numerical simulation. Geofluids 2020:1–34. https://doi.org/10.1155/2020/8818749

Liu C, Zhu ZD, Niu ZH et al (2021) Analysis of seepage characteristics of fracture network in rock mass. J China Three Gorges Univ 43:73–79

Neuman SP (2005) Trends, prospects and challenges in quantifying flow and transport through fractured rocks. Hydrogeol J 13:124–147. https://doi.org/10.1007/s10040-004-0397-2

Olsson R, Barton N (2001) An improved model for hydromechanical coupling during shearing of rock joints. Int J Rock Mech Min Sci 38:317–329. https://doi.org/10.1016/S1365-1609(00)00079-4

Peng SP, Meng ZP, Wang H et al (2003) Testing study on pore ration and permeability of sandstone under different confining pressures. Chin J Rock Mech Eng 22:742–746

Suzuki A, Watanabe N, Li K et al (2017) Fracture network created by 3-D printer and its validation using CT images. Water Resour Res 53:6330–6339. https://doi.org/10.1002/2017WR021032

Tao Y, Liu WQ (2012) An equivalent seepage resistance model with seepage-stress coupling for fractured rock mass. Rock Soil Mech 33:2041–2047

Waite ME, Ge S, Spetzler H (1999) A new conceptual model for fluid flow in discrete fractures: an experimental and numerical study. J Geophys Res-Atmos 1041:13049–13060. https://doi.org/10.1029/1998JB900035

Walsh JB (1981) Effect of pore pressure and confining pressure on fracture permeability. Int J Rock Mech Min Sci Geomech Abstr 18:429–435. https://doi.org/10.1016/0148-9062(81)90006-1

Wang L, Cardenas MB (2016) Development of an empirical model relating permeability and specific stiffness for rough fractures from numerical deformation experiments. J Geophys Res-Sol Ea 121:4977–4989. https://doi.org/10.1002/2016JB013004

Wang M, Chen YF, Ma GW et al (2016) Influence of surface roughness on nonlinear flow behaviors in 3D self-affine rough fractures: Lattice Boltzmann simulations. Adv Water Resour 96:373–388. https://doi.org/10.1016/j.advwatres.2016.08.006

Wang CS, Jiang YJ, Liu RC et al (2020a) Experimental study of the nonlinear flow characteristics of fluid in 3d rough-walled fractures during shear process. Rock Mech Rock Eng 53:2581–2604. https://doi.org/10.1007/s00603-020-02068-5

Wang SM, Tan C, Ma DH et al (2020b) Statistical simplification and discrete element analysis of seepage model for complex fracture network of dam foundation rock mass. IOP Conf Ser: Earth Environ Sci 570:1–13. https://doi.org/10.1088/1755-1315/570/6/062026

Xie LZ, Gao C, Ren L et al (2015) Numerical investigation of geometrical and hydraulic properties in a single rock fracture during shear displacement with the Navier-Stokes equations. Environ Earth Sci 73:7061–7074. https://doi.org/10.1007/s12665-015-4256-3

Xue L, Chen S, Shahrour I (2014) Algorithm of coupled normal stress and fluid flow in fractured rock mass by the composite element method. Rock Mech Rock Eng 47:1711–1725. https://doi.org/10.1007/s00603-013-0500-x

Yang TJ, Wang SH, Wang PY et al (2022) Hydraulic and mechanical coupling analysis of rough fracture network under normal stress and shear stress. KSCE J Civ Eng 26:650–660. https://doi.org/10.1007/s12205-021-0660-2

Zhang Z, Nemcik J (2013) Fluid flow regimes and nonlinear flow characteristics in deformable rock fractures. J Hydrol 477:139–151. https://doi.org/10.1016/j.jhydrol.2012.11.024

Zhou JQ, Hu SH, Fang S et al (2015) Nonlinear flow behavior at low Reynolds numbers through rough-walled fractures subjected to normal compressive loading. Int J Rock Mech Min Sci 80:202–218. https://doi.org/10.1016/j.ijrmms.2015.09.027

Zhou JQ, Hu SH, Chen YF et al (2016) The friction factor in the Forchheimer equation for rock fractures. Rock Mech Rock Eng 49:3055–3068. https://doi.org/10.1007/s00603-016-0960-x

Zhu HG (2012) Flow properties of fluid in fractured rock. Dissertation. Dissertation, China University of Mining and Technology (Beijing).

Zimmerman RW, Al-Yaarubi A, Pain CC et al (2004) Non-linear regimes of fluid flow in rock fractures. Int J Rock Mech Min Sci 41:163–169. https://doi.org/10.1016/j.ijrmms.2004.03.036